J Ther Eng, Vol. 12, No. 2, pp. 739−755, March, 2026

Journal of Thermal Engineering
Web page info: https://jten.yildiz.edu.tr
DOI: 10.14744/thermal.0001115

Research Article

Thermal gradients and ferrite formation in weld joints: A detailed study of temperature effects on microstructure and mechanical properties

Loay M. MUBARAK[1], Hussein M. AL-MRAYATEE[2], Ahmed Hashim KAREEM[3], Bassam Ali AHMED[4], Hasan Shakir MAJDI[5]

[1]*Department of Mechanical Engineering, College of Engineering, University of Diyala, Diyala, 32001, Iraq*
[2]*Institute of Technology-Baghdad, Middle Technical University, Baghdad, 10074, Iraq*
[3]*Department of Mechanical Techniques, Amarah Technical Institute, Southern Technical University, Basra, 44001, Iraq*
[4]*Department of Electromechanical Engineering, University of Technology- Iraq, Baghdad 10001, Iraq*
[5]*Department of Chemical Engineering and Petroleum Industries, Al-Mustaqbal University College, Babylon, 51001, Iraq*

ARTICLE INFO

Article history
Received: 11 March 2025
Revised: 24 June 2025
Accepted: 10 July June 2025

Keywords:
AISI 304 Stainless Steel TIG Welding; Ferrite Content; Phase Transformation; Weld Microstructure; Welding Heat Input

ABSTRACT

This study investigates TIG welding current variations effects on 4 mm thickness AISI 304 stainless steel joint welded using Argon gas, and this process impacts on ferrite composition, structural properties and joint strength. Ferrite content control must be managed properly to prevent hot cracking while ensuring both material strength and corrosion resistance because improper management leads to deficits during welding operations. A set of welding currents starting at 100 A progressed to 150 A and ending at 190 A created welds which delivered heat inputs of 6 J/mm, 9 J/mm and 11.4 J/mm. Welds under each condition received full inspection using metal structure analysis, scanning electron microscopy (SEM) along with Ferritoscope ferrite measurement, Vickers hardness analysis and mechanical strength testing. Data showed that a rise in heat intensity led to more ferrite formation starting from 4% at 100 A up to 9% at 190 A. The welds with 150 A heat application produced the optimal combination of mechanical properties since they contained 6% ferrite and displayed peak tensile strength at 689 MPa and mid-range hardness from 160–170 HV along with increased resistance to hot cracking. The welding current at 100 A produced a high hardness level of 170–181 HV in the weld but lost strength because of excessive ferrite content. Meanwhile the weld at 190 A exhibited lower strength and reduced hardness (150–157 HV) due to its excessive ferrite formation. Because of its ability to achieve superior microstructure with desirable austenite-to-ferrite ratio the weld using 150A heat input delivers optimal weld quality. The current investigation establishes quantitative assessments about heat treatment effects on AISI 304 TIG welds which distinguishes itself from previous research. The integration of Schaeffler diagram modeling with direct ferrite evaluations paired with SEM verification leads to a superior method for welding process prediction and enhancement.

Cite this article as: Mubarak LM, Al-Mrayatee HM, Kareem AH, Ahmed BA, Majdi HS. Thermal gradients and ferrite formation in weld joints: A detailed study of temperature effects on microstructure and mechanical properties. J Ther Eng 2026;12(2):739−755.

***Corresponding author.**
*E-mail address: louay_mohamed@uodiyala.edu.iq

This paper was recommended for publication in revised form by Editor-in-Chief Ahmet Selim Dalkılıç

INTRODUCTION

Researchers have extensively studied how temperature fluctuations affect ferrite content and structure formation in welded joints throughout welding metallurgy. The analysis of these effects leads to better weld mechanical properties since proper thermal management during welding affects ferrite phase development. García-García and Reyes-Calderón (2022) [1] evaluated how δ-ferrite composition affects the mechanical characteristics within austenitic stainless steel welded joint areas. Research showed that modifying δ-ferrite content within the HAZ area produced major alterations that affected weld properties regarding toughness and cracking resistance. The article published by Chukwuneke et al. (2022) [2] examines steel weld joint mechanical properties together with their thermal distortions through numerical methods. There was an investigation into how various heat amounts transform material structures through studies of weld metal structural alterations and Heat Affected Zone transformations. Perpetual research has shown that changing thermal gradients affect ferrite preservation deeply yet controlled welding configurations reduce weld distortion levels effectively.

Vasantharaja and Vasudevan (2019) [3] investigated how TIG and A-TIG welding methods affect the microstructure together with mechanical properties of ferritic-martensitic (RAFM) steel welds. The research showed that welding temperatures as well as cooling speed after welding affect the ferrite composition and mechanical property development of welded materials. Yanfa Han et al. (2025) [4] research analyses the MP-GMAW of ZGMn13Mo/A514 using the microstructure, mechanical properties, residual stress, and distortion analysis. In the weld metal, there are γ-austenite and Cr-rich δ-ferrite phases were identified and the martensitic transformation in the HAZ of A514 was observed. Tushar Sonar et al. (2015) [5] paper presented a critical evaluation of dissimilar welding of FMS and ASS using GTAW technique with focus on weldability problems including hot cracking, cold cracking and δ-ferrite formation. It also describes influence of the welding parameters, filler materials and post-weld heat treatment on the microstructure and mechanical characteristics of joints. Fei et al. (2020) [6] examined how post-weld heat treatment influenced deep penetration autogenous TIG-welded dissimilar joints from the viewpoints of their microstructure and mechanical properties. Examination of controlled post-weld thermal cycles enabled HAZ ferrite content adjustment that resulted in enhanced strength together with ductility of welded joints. Queiroz et al. (2020) [7] conducted research on how external magnetic fields affect TIG-welded joints both structurally and mechanically. The fusion zone received both thermal influence and magnetic field exposure that modified ferrite distribution and stability patterns. Li et al. (2019) [8] conducted experimental research that assessed simulated welding thermal cycles for studying microstructural and mechanical properties in austenitic stainless steel with high nitrogen content through its large-grained thermal-impacted area. Maduraimuthu et al. (2012) [9] studied how activated flux affected modified 9Cr-1Mo steel weld joints through tests on their microstructure along with their mechanical properties and residual stress measurements. Heat input and cooling rates during welding temperature behavior led to changes in ferrite content that determined the weld mechanical performance. The research conducted by Raj et al. (2024) [10] investigated the thermal aging impacts on the tensile characteristics alongside metallurgical properties of stainless steel weld joints. The research established that ferrite content significantly affects weld mechanical properties and thermal aging affects ferrite stability through post-weld treatments that enhance overall performance. Zmitrowicz et al. (2021) [11] research uses linear welding energy to analyze its effects on ferrite content throughout HAZ and weld zone of duplex stainless steel materials. The study shows that higher linear welding energy levels led to increased ferrite content in the HAZ regions but the greatest WM ferrite percentage. Noga et al (2024) [12] study focuses on how multiple welding techniques (MIG, TIG, PAW, and EBW) changing the microstructure structure alongside mechanical characteristics of duplex stainless steel welds. The paper explains how heat input rates and cooling conditions affect ferrite crystal structure and arrangement that determines weld mechanical properties. Mohammed et al. (2017) [13] research evaluates microstructural mechanical and corrosion effects that various welding heat inputs produce in duplex stainless steel fusion areas. The weld metal requires slower cooling rates when heat input is high causing more austenite to form and reducing the ferrite amount. Higelin et al. (2022) [14] research analyzes methods to manage ferrite content within the HAZ regions of plex stainless steel welded areas. This investigation studies the impact of various welding factors on austenite-to-ferrite transformation in welding operations that modifies weld mechanical behaviors. Wang et al. (2023) [15-19] article examination the thermal mechanical welding operations which modify welded joint microstructure and mechanical characteristics. The study examines the connection between thermal cycling effects on ferrite pattern and its distribution that modifies weld properties regarding strength and ductility.

The novelty of this research lies in its detailed investigation of the impact of varying TIG welding currents (100 A, 150 A, or 190 A) on the microstructure and overall performance of AISI 304 stainless steel welds. This study examines the critical aspect of regulating ferrite levels in welded joints, as it influences both the material's strength and toughness. A significant improvement is the utilization of Schaeffler diagrams in conjunction with direct ferrite content measurements and SEM analysis to refine process prediction and enhancement. The research concludes that 6% ferrite, achieved with 150 A of heat input, optimally balances tensile strength, toughness, and fracture resistance. The optimal environment for welding enhances the

material's strength and mitigates the danger of hot cracking, making it particularly advantageous for components susceptible to corrosion. It examines the impact of welding on austenitic and ferritic phases, educating readers about the microstructure and characteristics of welded joints. The microstructural control of δ-ferrite is crucial for maintaining strength and corrosion resistance in austenitic stainless steel AISI 304 welds, which are used in pressure vessels and piping systems. Previous research has not adequately explored the correlation between heat input variations and ferrite development and austenitic weld mechanical properties, such as hardness, tensile strength, and phase transformations. This paper addresses these shortcomings by examining TIG welding current variations (100 A, 150 A, 190 A) to control heat input and measure its effects on structural properties and mechanical outputs. The research also establishes a connection between metal phase modifications and tensile strength measurements and hardness data, extending from weld core areas to heat-affected region sections. The optimal combination of mechanical characteristics is found at 150 A / 6% ferrite.

EXPERIMENTAL PROCEDURE

Investigation Materials

Two AISI 304 austenitic steel plates employed in the testing had 4 × 1000 × 2000 mm dimensions. Table 1 shows the base steel chemical composition according to the acceptance certificate. ER 308 was the TIG filler welding material that was utilized. Table 2 shows the TIG filler chemical composition. The welding joint design employed a single V-shape with a 60 degrees angle, as specified by the AWS A2 standard. When welding was done, a brace was placed on both ends of the specimen to prevent it from becoming deformed. This was necessary since the heat created by the welding may cause deformation, and the specimen was considered to be a solid or massive material.

The three samples final welding settings were applied based on preliminary technical testing on the specimens under the specified dimensions. The technological testing primary objective was to create welded joints that met the criteria and did not have any welding flaws. After testing, the final joints welding parameters are provided in Table 3, 100% Ar as shielding gas was used.

Microstructure Examinations

An Olympus GX51 light microscope was used to analyze welded joints microstructure. The samples were cold mounted in a Spruers Fixi Form container using Struers ‹EpoFix epoxy adhesive. The samples that were generated in this manner were subsequently processed on sandpaper with 320 - 1500 grain. Polishing purposes utilized by diamond suspensions. OP-S polishing suspension from Struers was used to complete the polishing process. In order to show AISI 304 stainless steel microstructure, the specimens electrolytically etched in 10% nitric acid at 1.5 V voltage for 20 s at room temperature. A HITACHI SU-70 scanning electron microscope with an attachment chemical composition (EDS) microanalysis was used to conduct scientific study on a micro scale. The quantitative metallography approach and the MPD-100 ferritoscope were used to conduct tests that measured the ferrite content in AISI 304 welds and base material. The ferritoscope employs a technique that is based on substance magnetic characteristics measuring. The material magnetic permeability being evaluated is used to determine ferrite present quantity. The findings are shown as percentages.

Table 1. AISI 304 chemical composition (% by weight)

Fe	C	Si	Mn	S	P	Ni	Cr	N
Bal.	0.07	1.00	2.00	0.015	0.045	9.84	18.93	0.10

Table 2. ER 308L electrode chemical composition (% by weight)

Fe	C	Cr	Si	Mn	S	Mo	P	Cu	Ni
Bal.	0.02	20.1	0.44	1.6	0.02	0.03	0.02	0.11	9.2

Table 3. TIG with ER 308L electrode welding parameters

No.	Filler Dia.	Current (A)	Voltage (U)	Welding Speed (Vs)	Shielding Gas	Flow rate (L/min)	Tungsten Electrodes
1	1.6 (mm)	100 A	12 V	140 (mm/min)	Argon	15	2% Thorium
2		150 A					
3		190 A					

Mechanical Measuring Procedure

Acquired joints mechanical tests comprised a uniaxial tensile test, a bending test, and a hardness assessment using the Vickers technique. For uniaxial tensile samples, the measuring base had 25 mm a width, 4 mm thickness, and 60 mm length. Three samples were obtained from each welded joint, and tensile tests were conducted on them [19]. MTS Criterion C45 testing machine was used to conduct the tests. Bending tests were performed on flat pieces that were 300 × 25 × 4 mm dimension [20]. The Vickers hardness test (HV) was conducted on the base metal (BM), heat affected zone (HAZ), and weld metal (WM) at ambient temperature, in accordance with ASTM E92-82. A diamond indenter was employed with a load of 10 Kgf and a dwell period of 15 seconds. To provide clear visualization of the data in each of the three zones, three measurements were conducted inside each zone. The objective of the microhardness tests is to determine the hardness of the material in each region, thereby providing insights into the microstructure and mechanical properties of the welded joint [21]. Measurements were done in four measuring lines that ran through each sample base material, weld, and HAZ. Hardness measurements taken in this manner were used to create a two-dimensional graphic depicting the hardness profiles in welded joints. Fig. 1 shows the dimensions of tensile test samples according to the ASTM E8 standard [22]. Fig. 2 below illustrates the welded joint assessment procedure and sequence graphically.

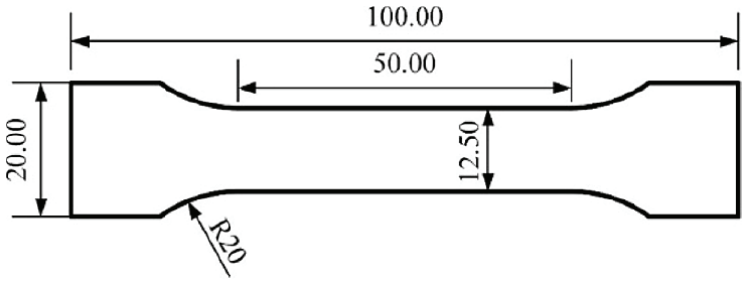

Figure 1. Schematic of tensile test specimen size and dimensions. [Refer to ASTM E8 standard, adapted in accordance with [22].

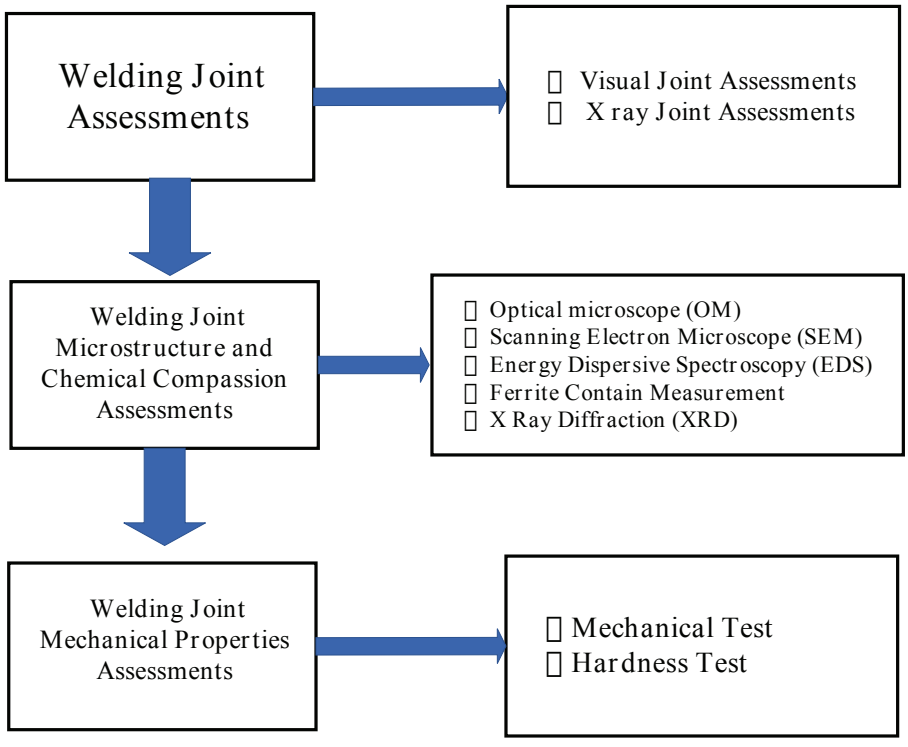

Figure 2. Welding joint assessment procedure.

Schaeffler Diagram Ferrite Calculation

To enhance mechanical qualities and corrosion resistance, ferrite-forming elements like as Mo, W, Si, Ti, Nb, and V are employed as alloying additions. When included into steel, they also constrict the stability range of the γ phase, often reducing the propensity of austenite to precipitate phases such as σ, Laves, χ, and others. To preserve the single-phase γ structure, it is essential to incorporate an ideally elevated Ni content into the steel. Otherwise, the steel may acquire a dual-phase structure: austenite and metastable ferrite. Earlier studies indicates that minimal presence of δ ferrite inhibits hot cracking in austenitic steels, with a concentration of 1–6% effectively preventing hot cracking in welded austenitic steels and decreasing the crack propagation rate during stress corrosion cracking [23,24].

The amount of ferrite in the weld is determined by its chemical composition. Alloying elements in austenitic steels are classified as ferrite-forming and austenite-forming elements. The influence of chemical composition on microstructure and solidification is denoted by chromium and nickel equivalents. The chromium equivalent is the aggregate of chromium content and ferrite-forming components, each weighted by coefficients that denote their influence on the relative proportion of ferrite in relation to chromium. Fig. 1 presents a Schaeffler diagram, outlining the areas where the weld structure of corrosion-resistant steels is exhibited, measured in nickel and chromium equivalents [25, 26]. This graphic is a useful tool for evaluating the effects of integrating filler metal into the base material of the joint, enabling computation of the ferrite content in the joint.

RESULTS AND DISCUSSION

Welding Zone Microstructure Analyses

Figure 4 (A) demonstrates the raw AISI 304 steel material microstructural composition through microscopic analysis. AISI 304 stainless steel exists as an austenitic steel structure with its fundamental crystal arrangement as face-centered cubic (FCC) lattice when operating at room temperature. The image demonstrates a uniform arrangement characteristic of austenitic phase typical in the material structure. Equiaxed (roughly spherical) grains appear round in shape as light areas where their microstructure maintains homogeneity. The metal exhibits ductility along with toughness due to its crystal arrangement that serves as a characteristic feature of 304 stainless steel.

The dark lines that separate grain areas indicate grain boundaries in the material structure. Because crystallographic orientations differ in these locations, they form interfaces. The material's mechanical properties depend significantly on grain boundaries because they influence strength, ductility, and corrosion resistance. These boundaries prevent dislocations from moving because of their high-angle nature. The morphology in Figure 4 (A) contains various circular or undefined dark shapes that most likely consist of non-metallic inclusions together with second-phase particles. Materials' strength and toughness typically suffer due to manufacturing process-related factors that create defects in the material. Any elongated or distorted grain appearance in base metal morphology tends to suggest plastic deformation linked to dislocation motion. The dislocations formation occurs predominantly in materials that go through processing stresses either from rolling or drawing treatments. Under certain

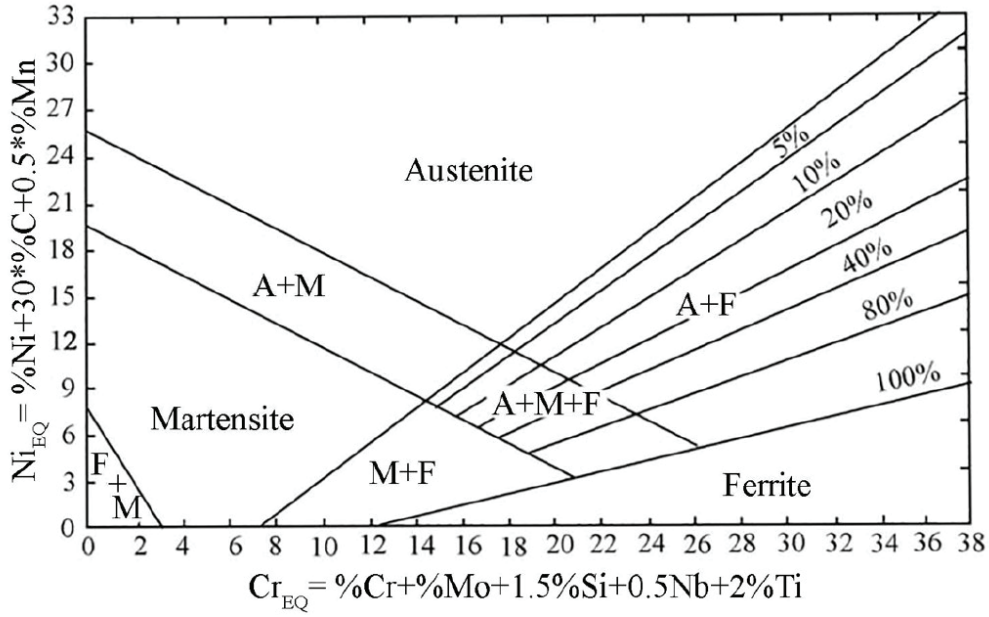

Figure 3. Schaeffler Diagram used for determining weld structure phases and ferrite content. [Adapted from Kou [26]].

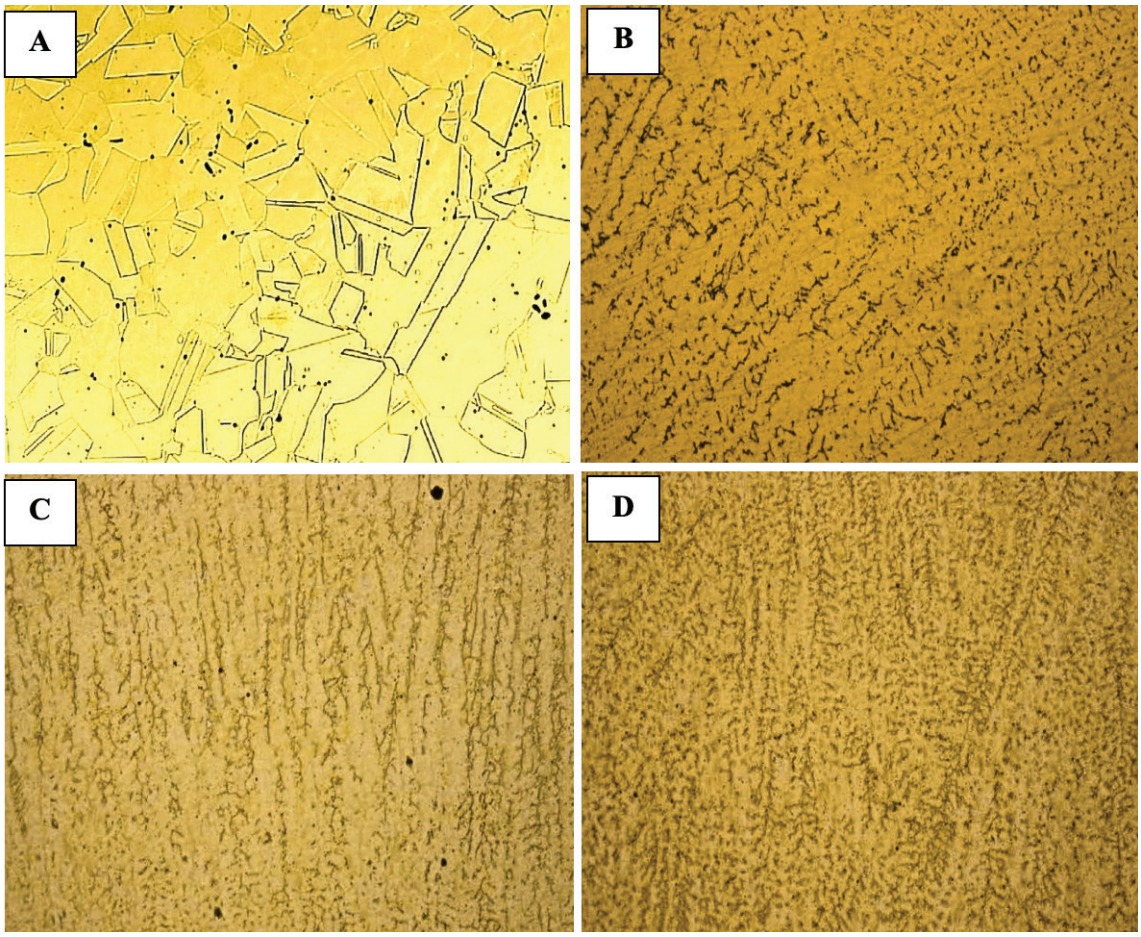

Figure 4. Base metal and welding zone microstructure (A) base metal (B) 190 A welding current (C) 150 A welding current (D) 100 A welding current.

conditions, AISI 304 stainless steel main composition consists austenite with small ferrite traces that is another steel phase with body-centered cubic structure. Small ferrite amounts exist within the typical AISI 304 microstructure despite the normal austenitic phase. Phase transitions in steel occur when alloys modify the steel or when cooling procedures drain heat from the material. The microstructure of AISI 304 stainless steel structures serves as its main defense against corrosion effects. Austenitic homogeneity in AISI 304 structures protects the material from general corrosion and pitting failure. Chloride-rich solutions can increase corrosion susceptibility in inclusions and disturbed areas near grain boundaries. High heat input conditions during welding produce distinctive features in austenitic stainless steel weldments, such as the dendritic pattern with networked ferrite formations. The fusion zone (FZ) is formed from different phases during welding. Primary Austenitic Solidification with Ferrite ($\gamma + \delta$) emerges as the product of high heat input when using 190 A fusion zone (FZ). Under austenitic-ferritic solidification mode, the weld region forms dendritic austenite grains. The presence of δ-ferrite phase prevents hot cracking during welding austenitic stainless steel. Elevated temperature difference promotes columnar dendrite development, while composition segregation and cooling rate determine dendrite formation. AISI 304 welds have a ferrite content proportion of 5-12%, improving cracking resistance. However, toughness and ductility suffer when δ-ferrite amount exceeds 10%. This process creates a heterogeneous element distribution, potentially causing corrosion resistance problems in local areas. The observed microstructure matches austenitic stainless steel weldments even though it displays differences in comparison to weldments using higher heat inputs. The main solidified component in the weld operates as austenite (γ) phase while developing dendritic shapes stretching from the fusion boundary. Moderate welding current welds (150 A) dendritic structures appear finer and more organized than those of high-heat input welds like the 190 A welds because of their coarser structure. Less δ-ferrite remains in the interdendritic areas of welds affected by moderate cooling rates than in welds undergoing extensive cooling. δ-ferrite appears as a dark network of bones throughout the image because it developed within the interdendritic structures. The welds possess enough ferrite to avoid hot cracking despite having less compared to high-heat input welds. Metals made of ER308 include a specific design feature

that maintains δ-ferrite at ~5–8 % levels for inhibiting cracks. The moderate dendritic patterns in the fusion zone mostly show columnar dendrites that extend with the direction of thermal dissipation. The weld dendrites of lower heat input applications tend to appear shorter along with finer dimensions than their high-heat input counterparts (190 A) thus resulting in enhanced mechanical characteristics. The resistance of material against corrosion improves when cooling occurs at moderate levels. The weld joint done with 100 A low current power appears in Fig. 4 (D) as the fusion zone (FZ). The decreased heat exposure during welding affects basic characteristics of weld quality. An application of 100 A welding current creates reduced heat input that results in accelerated cooling during material welding. During this process the dendrite formation mechanism and ferrite distribution as well as phase transformation patterns are affected. The Austenite phase is the main microstructural phase in weld welding, with a faster cooling rate and lower ferrite amounts due to decreased heat input. Dendrites become denser due to heat escape, and in low heat input welds, dendrites remain small and less elongated. Weld metal solidification occurs rapidly, reducing grain growth and increasing mechanical strength. The lower distribution of Cr, Ni, and Mo enabling elements enhances corrosion protection. Ferrite crystal formation is less pronounced in 100 A heat input welding compared to 150 A and 190 A heat inputs, leading to an upward trend in ductility and a marginal rise in hot crack formation. The weld metal exhibits 3–5% ferrite crystals, with a crystal count below the minimum breaking threshold. The analyzed joints of the three samples exhibit mostly austenitic microstructures, with the presence of delta ferrite precipitates. The welds exhibit cellular and dendritic microstructures, whilst the weld axes have a uniform structure. Columnar dendrites exhibited both primary dendritic arm spacing (PDAS) and secondary dendritic arm spacing (SDAS). A comparable microstructure was seen in Kulkarni's work. [27]. Because the temperature gradient to solidification rate ratio is reduced, dendritic microstructure is present at the fusion lines and equiaxed inside the weld line [28]. A refined equiaxed dendritic morphology was seen in the center of the fusion zone as a result.

Welding Zone Ferrite Content Measurements

Ferrite content was measured using both a magnetic method using a Ferritoscope and metallographic technique. After weld joint dilution calculations based on the resulted joint geometry dimensions, The chromium equivalent (Creq) and nickel equivalent (Nieq) were calculated from the chemical composition of AISI 304 steel and ER308 austenitic steel (filler metal). The welding zone nickel and chromium equivalents listed in Table 4 below for the three welding samples. The calculated values revealed the expected ferrite content in the weld, derived from the Schaeffler diagram (Fig. 3), which indicated a delta ferrite concentration value in. The results reflected the Creq/Nieq ratio effects on solidification mode and the joint resulting microstructure.

Table 4 reveals the impact of welding input heat on Creq and Nieq. High heat inputs cause slower cooling, causing chromium and molybdenum alloying elements to separate differently across the fusion zone, reducing their uniform distribution. Heat exposure in the heat-affected zone results in Cr23C6 precipitation, depleting chromium resources. Lower temperatures lead to decreased Creq concentration, resulting in poor corrosion resistance. Higher heat inputs cause chromium depletion from grain boundary areas, reducing Creq content in the fusion zone. [29]. The alloying elements have less time to segregate because of rapid cooling that happens when the heat input remains low. The weld corrosion resistance remains strong because minimal carbide precipitation forms when heat input stays low. Reducing the heat input along with fast weld cooling produces better resistance to pitting and crevice corrosion by creating higher Cr_{eq} composition. The heat input had the same effects on the $Ni_{eq,}$ the weld pool cooling becomes slower when high heat inputs are applied thus causing an increase in carbon (C) and nitrogen (N) concentration. The Ni_{eq} concentration becomes higher when carbon accumulates nickel properties and converts the weld metal to an austenitic state. Higher Ni_{eq} pushes the weld toward increased stability of γ-phase. The excessive austenite formation becomes more likely as cooling takes place too slowly. Fast weld cooling occurs when applying low heat that minimizes the carbon (C) and nitrogen (N) influence. The rapid weld cooling produces lower Ni_{eq} equilibrium content and increases the ferritic or martensitic phases in low alloy stainless steel weld metal. The weld region with diminished Nieq exhibits unstable austenite structures due to rapid cooling rates, which foster the production of ferrite or martensitic phases, thereby impairing ductility and toughness. A medium or diminished Nieq value fosters microstructural equilibrium, enhancing material properties during particular welding procedures. Table 5 below show summary heat input effects on Cr_{eq} and Ni_{eq} and welding zone geometry in stainless steel welding [30].

Table 4. Three welding samples Creq, Nieq, Creq/Nieq ratio, and calculated FN

Welding current	Input heat	Cr_{eq}	Ni_{eq}	Cr_{eq}/Ni_{eq} Ratio	FN%
100 A	6 J/mm	18.85	12.84	1.46	4
150 A	9 J/mm	18.21	11.66	1.56	6
190 A	11.4 J/mm	17.83	10.16	1.75	9

Table 5. Heat input effects on Cr_{eq} and Ni_{eq} and welding zone geometry

Parameter	Higher Heat Input (190 A)	Moderate Heat Input (150 A)	Lower Heat Input (100 A)
Weld Geometry	Wider weld bead, deeper penetration, larger HAZ, potential distortion	Balanced bead size and penetration, moderate HAZ	Narrower weld bead, shallower penetration, smaller HAZ
Cr Equivalent (Cr_{eq})	Decreased due to chromium depletion in HAZ, lower corrosion resistance	Balanced Cr_{eq}, good corrosion resistance	Higher Cr_{eq}, better uniformity and corrosion resistance
Ni Equivalent (Ni_{eq})	Higher Ni_{eq} (better austenite stability) but risk of excessive austenite	Moderate Ni_{eq}, balanced austenite and ferrite phase stability	Lower Ni_{eq}, possibly more ferrite/ martensite, reduced austenite

The Ferritoscope ferrite contains measurements results of the three samples were very close to the calculated values, with a little error percentage, Ferritoscope detects the magnetic ferrite phase to directly determine the ferrite content in stainless steel welds. The measurement procedure of Ferritoscope depends on their ability to detect differences in ferrite and austenite magnetic properties. The ferrite content measured by Ferritoscope shows minimal differences from diagrams generated by the Schaeffler Diagram because it perfectly matches overall weld phase distributions which derive mainly from Cr and Ni elements. Fig. 5 below illustrated the values of ferrite percentage between the calculated values from Schaeffer diagram and the ferrite percentage measuring by ferrometer. The Schaeffer Diagram is derived from an analysis of the material›s chemistry, whereas the Ferrometer provides a measurement pertaining to the material›s magnetic. The Ferrometer is often a superior instrument for assessing ferrite when measured directly from the welded metal, as it does not rely on the tool›s estimations of the metal›s composition. The ferrometer is superior at identifying genuine alterations in the microstructure caused by welding, such as rapid cooling rates, whereas the Schaeffer Diagram neglects these variables during cooling and may yield divergent outcomes.

The research assesses FZ microstructure development through three heat input parameters at 100 A, 150 A, and 190 A. The manuscript details the changes that affect key microstructural aspects from dendrites to ferrite content together with grain growth and elemental distribution and sensitization levels and toughness alongside material properties. The authors present in Table 6 important insights regarding the trade-offs regarding heat input and microstructural evolution and performance attributes for optimized welding process control. Through FZ microstructural observation after heat application welders understand how welding metallurgy affects material strength during high-stress operation.

Hot cracking resistance strengthens through ferrite because these particles act as impurity traps that collect sulfur and phosphorus atoms around the grain boundaries.

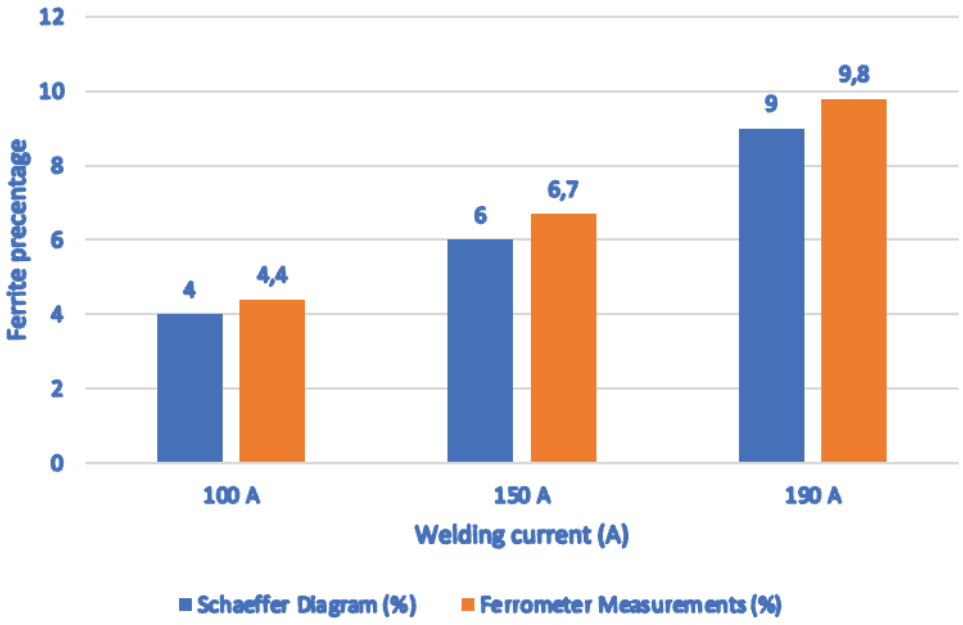

Figure 5. Ferrite percentage measurements differences between Schaeffler diagram and Ferritoscope instrument.

Table 6. Fusion zone (FZ) microstructures comparison based on heat input effects

Feature	100 A (Low Heat Input)	150 A (Moderate Heat Input)	190 A (High Heat Input)
Heat Input	Low	Moderate	High
Cooling Rate	Fast	Moderate	Slow
Dendritic Structure	Fine dendrites (best strength)	Moderate dendritic structure	Coarse dendritic structure (weaker toughness)
Ferrite Content (δ-Ferrite)	Low (~3-5 %) - higher hot cracking risk	Moderate (~5-8 %)	Higher (~8-12 %) - best crack resistance
Grain Coarsening	Minimal - best toughness	Moderate - balanced toughness & strength	Significant - lowers toughness
Elemental Segregation	Minimal - best uniformity	Moderate - acceptable segregation	High - risk of localized corrosion
Sensitization (IGC Risk)	Very Low (best corrosion resistance)	Low - still good corrosion resistance	High - prone to intergranular corrosion (IGC)
Crack Resistance	Moderate - risk of solidification cracking	Best balance between strength & cracking resistance	Best resistance to hot cracking
Mechanical Properties	Best strength & toughness due to fine grains	Balanced mechanical properties	Lower strength & toughness due to coarse grains
Corrosion Resistance	Best resistance due to minimal carbide precipitation	Good - but requires control of heat input	Lower - due to carbide precipitation & segregation

Because of its low ferrite content (4 %) at 4 %, the weld remains susceptible to solidification cracking especially when performing welding under high-restraint conditions. A maximum hot cracking resistance is achieved when standard ferrite content ranges from 5 % to 10 %. Lower ferrite values below 5 % favorably affect both ductility and impact toughness thus improving weld sudden load performance. Higher flexibility emerges from the weld›s austenite-intensive structure yet its reduced strength outweighs the strength obtained from greater ferrite content. The reduction of ferrite content usually improves machining outcomes in particular applications. Weld metal with 4% ferrite content displays the most effective pitting corrosion and crevice corrosion resistance while keeping sufficient corrosion levels [31]. The requirement of chloride ions in solution calls for weld metals to contain less ferrite in order to avoid localized corrosion affecting ferrite regions. Ferrite exhibits ferromagnetic properties that contrast austenite because ferrite operates as a ferromagnetic material yet austenite operates as paramagnetic. Refraining from magnetism is possible in weld metals with 4% ferrite content making this material appropriate for magnetic field-sensitive applications. According to the experts, the incorporation of ferrite provides weld metals with dual advantages: high-temperature oxidation protection plus grain boundary sliding control. Welds starting service above 600°C result in excessive ferrite formation exceeding 10%. Subsequent ferrite transformation creates brittle sigma (σ) phase that weakens the weld toughness. Weld materials with 4% ferrite content stay stable at high temperatures because they develop minimal sigma phase presence [32]. The mechanical properties and resistance to cracking along with corrosion performance of the weld zone depend on its 6 % ferrite content. Ferrite in a weld metal absorbs harmful elements like S, P and Si which prevents hot cracking by combining with 6% ferrite providing a balance that improves hot cracking resistance compared to using 4 % ferrite metal at 100 A. The fracture risks decrease proportionally with weld ferrite content under 5% so this enhanced level ensures stronger structural performance. Weld›s toughness and ductility are slightly lower than austenitic welds due to an increase in ferrite content. However, the appropriate ferrite content leads to increased mechanical strength and thermal stability, resulting in greater mechanical load resistance. Higher ferrite content reduces corrosion resistance, but it remains in acceptable levels. The resistance to pitting corrosion in chloride environments is slightly diminished compared to low ferrite and higher ferrite welds. Stress corrosion cracking and intergranular corrosion exhibit stable resistance. Ferrite›s magnetic property differs from austenite, acting ferromagnetic but remaining paramagnetic. The weld with 6% ferrite shows improved magnetic properties but non-magnetism. Ferrite also enhances resistance to high-temperature oxidation and grain boundary sliding. Welds with 9% ferrite have a low probability of developing sigma phase due to increased formation risk. 9% ferrite content improves cracking resistance, mechanical strength, and corrosion resistance. Ferrite plays a crucial role in solidification cracking prevention by taking in segregating elements like S and P. Welds with 9% ferrite have limited hot cracking risks and superior resistance against solidification issues. The elevated ferrite level in the weld metal boosts mechanical strength and prevents deformation [33]. During service operations, Ferrite produces fewer thermal expansion effects than austenite

because it›s thermal expansion coefficient stands lower. The corrosion resistance decreases as ferrite levels rise above 10 % since ferrite shows reduced resistance against pitting and crevice corrosion than austenite. With a ferrite, content of 9 % the weld material shows increased vulnerability to chloride-induced localized corrosion especially in marine settings when contrasted with welds containing lower amounts of ferrite. Most applications show suitable performance in terms of general corrosion resistance. The material composition of ferrite contains magnetic properties and austenite demonstrates paramagnetic responses. The weld metal maintenance with 9% ferrite content possesses reasonable ability to attract magnets but fails to meet non-magnetic application requirements. The presence of ferrite strengthens the material at high temperatures yet the material becomes brittle when the temperature reaches above 600 °C where it transforms into the sigma (σ) phase. Welds containing 9 % ferrite carry a higher risk of sigma phase formation than welds that have 4–6 % ferrite mostly because they both affect the toughness and impact strength during extended exposure to elevated temperatures. The weld needs to have ferrite content below 8 % when it must handle prolonged exposure to high temperatures.

Welding Zone SEM Analyses

SEM plays an essential role in understanding changes in microstructures across TIG-welded 304 stainless steel joints as the researcher varies heat input levels from 100 A to 150 A and 190 A. Through SEM examination, detailed observations of weld metal structures, which show important information about the distribution of austenite and ferrite along with grain features and interdendritic patterns, can gain. Knowledge of these features leads to effective evaluation of solidification behavior and hot cracking susceptibility along with mechanical strength and corrosion performance assessments. The evaluation of microstructural details through SEM analysis enables optimal ferrite content determination alongside reliability enhancement and failure prevention in service applications across different welding current settings. Fig. 6 below illustrated the three welding zones SEM morphology [34].

An SEM micrograph from Fig. 6 (A) at 100 A shows that the weld zone consists of dendritic austenite with interdendritic

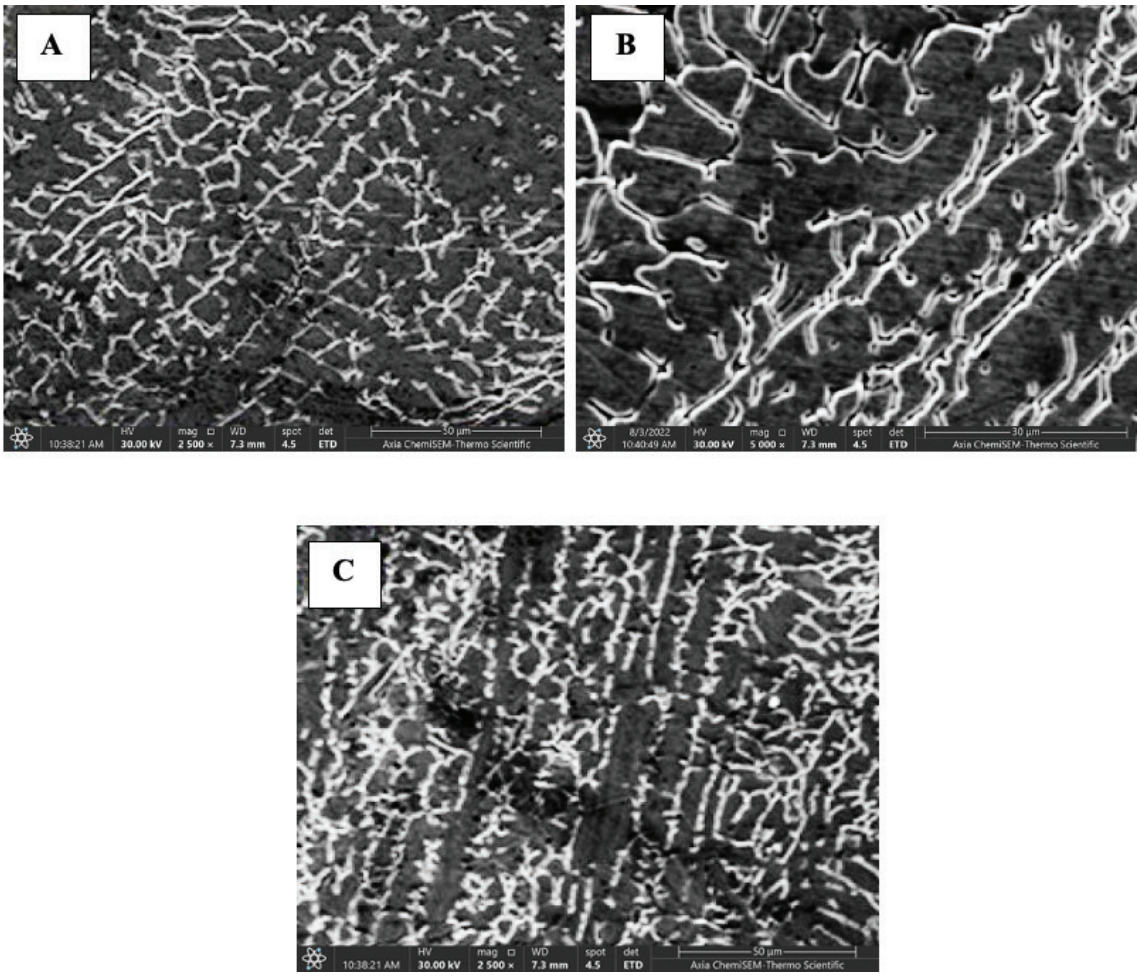

Figure 6. Welding zone SEM morphology (A) 100 A, (B) 150 A, and (C) 190 A.

ferrite that contains 4 % ferrite content. The combination of nickel (Ni) and carbon (C) elements in ER308 filler material stabilizes austenite. The dendritic formation indicates austenitic solidification that produced ferrite throughout interdendritic regions. The SEM image reveals the web-like bright structure as δ-ferrite that occurs between interdendritic boundaries. The weld solidified through an Austenite + Ferrite (AF) mode based on its 4 % ferrite content since austenite formed first then interdendritic ferrite appeared later. The segregation of Cr (chromium) and Mo (molybdenum) ferrite stabilizers produces ferrite in the metal structure. The minimum allowable ferrite amount in stainless steel welds stands at 3 % meaning the examined weld contains a near minimum concentration of ferrite. While the ferrite phase defends against solidification, cracking it exists at a limited 4 % level that may raise the susceptibility to hot cracking under high restraint. The low ferrite content provides excellent corrosion resistance along with ductility however; it reduces the hot-cracking resistance slightly.

SEM image in Fig. 6 (B) shows the weld metal microstructure at 150 A. The weld metal shows two distinct microstructures of austenite (γ-phase) as main phase and interdendritic δ-ferrite that strongly affects the weld properties. Dark areas viewed in the SEM image represent the γ-phase that is known as austenite. The austenitic phase exists as the major matrix component because nickel (Ni) from the ER308 filler metal stabilizes this phase. Austenite turned into the first solid phase during the process before ferrite developed between the dendrites. δ-ferrite exists as a bright network structure throughout the interdendritic spaces according to the SEM image. An enhanced welding current to 150 A creates more heat input that allows grain development and slows down cooling which helps stabilize additional ferrite. The weld obtained through 6 % ferrite content contains slightly elevated ferrite quantities than lower-amperage welds (100 A with 4 % ferrite) and thereby presents increased advantages for crack prevention. The weld zone microstructure at 190 A is depicted in Fig. 6 (C) through an SEM micrograph. The combination of high welding current (190 A) with 9 % ferrite percentage in the microstructure produces a higher ferrite fraction than welds forged with 100 A or 150 A welding current. The mechanical as well as corrosion behavior of the weld receives major modification through this change. In the SEM image, the dark areas represent austenite (γ-phase) that makes up the main structure of the material. Austenite receives stability from carbon (C) and nickel (Ni) while having ferrite remain present due to chromium (Cr) segregation. The region showing network-like brightness represents δ-ferrite while its percentage in this weld reaches 9 %. A welding current of 190 A produces elevated heat input that generates a slower cooling process during which ferrite can stabilize to higher percentages. The formation of Austenite + Ferrite (AF) solidification results in improved crack resistance according to this characteristic [35].

Welding Joint Hardness Profile Analyses

Testing the 304 stainless steel alloy TIG welds hardness profile attributes decisive value to the determination of structural mechanical behavior along with service duration. The combination of material strength and the resistance to wear and tendency to develop cracks can be measured

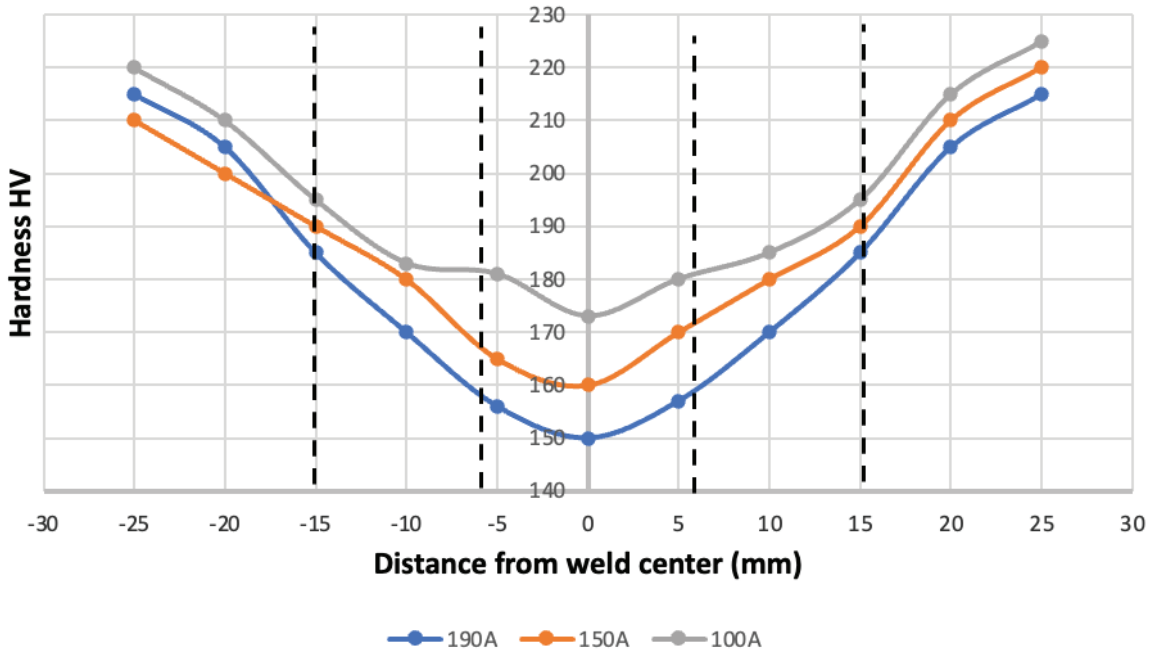

Figure 7. Hardness profile cross the welding joints.

through hardness tests. The testing method provides essential data that evaluates welding procedure outcomes and detects temperature inputs and thermal cooling rates and the processes within weldment metal and heat-affected areas [36]. Hardness assessment from end to end of the weld joint enables welding engineers to observe uniform structure patterns which in turn extends service duration and preserves component strength under operational loads. Building quality control systems using engineering requirements needs this evaluation method. Fig. 7 below represent the hardness profile of the three welding samples according to the welding current.

The base metal hardness demonstrates minimal change and persists within a range of 210 to 220 HV on the graph. The measurement for 304 stainless steel shows typical characteristics for an annealed state (austenitic structure). The welding current type has no effect on the hardness of the base metal because the material maintains identical composition and microstructure. The welding zone at the center of the graph displays reduced hardness levels whereas the intensities of hardness vary between the different welding currents. The gray line shows 100 A welding with the peak hardness degree of 170-181 HV across the welding zone. The formation of a refined microstructure occurs because of the reduced heat input that allows swift cooling of the material. The welding zone of the 150 A process (Orange line) exhibits peak hardness of 160-170 HV though it falls below the first welding joint's values. The 150 A heat input pace produces reduced microstructural cooling which enables the formation of a high 6% ferrite content. Weakening of material happens because ferrite exhibits decreased hardness compared to austenite and 190 A (blue line) produces the lowest peak hardness level which reaches 150-157 HV. The heat input generated from maximum welding current slows down the cooling process until 9% ferrite finally forms. Ferrite shows significantly lower hardness than austenite thus causing the welding area hardness to drop. The HAZ hardness gradually falls when moving away from the weld center and eventually reaches a similar level as the base metal. The HAZ hardness drop occurs because the cooling rate is slower than the base metal, allowing for more time for grain growth and diffusion of phases. when welding with 100 A (gray Line), The hardness in the HAZ drops to around 181-195 HV compared with the base hardness, which is still higher than the welding zone due to the relatively fine-grained microstructure resulting from faster cooling. 150 A welding current (Orange Line) shows hardness drops more significantly, stabilizing around 165-190 HV, as the cooling rate is slower, leading to larger ferrite and a more coarsely-grained microstructure. 190 A (Blue Line) HAZ hardness drops to around 156-185 HV because of the largest ferrite content and the coarser microstructure. The study results illustrated the influence of ferrite on the assessment of welded joint characteristics. Hardness measures diminish with an increase in ferrite, since ferrite is inherently softer than austenite. Conversely, the weld structure exhibits elevated hardness at 4% ferrite and 100 A, attributable to its substantial austenite composition. An elevated ferrite percentage of 6% (150 A) results in diminished hardness due to the augmented ferrite amount, while the maximum ferrite content of 9% achieves 190 A, yielding the softest weld zone. Table 7 below summarizes the contrast among these three joints and their correlation with the ferrite percentage.

Welding Joint Tensile Test Analyses

Notably, increasing the welding current had a positive effect on the strength of the welds with sample 2 with 150 A and very bad effects with sample 3 with 190 A. For instance, when welding with ER308, and 100 A welding current in sample 1, the tensile test recording 662 MPa, the strength increased to 689 MPa as the current was increased to 150 A. and reducing again to 677 when welding with 190 A, these results indicate that higher welding currents not always can lead to stronger welds. 100 A weld joint exhibits only 4 % ferrite composition. The microstructure mostly contains austenite together with a minor ferrite amount. The welded area strength derives from austenite because its hard properties surpass ferrite properties. For that the weld joint need a specific ferrite percentage to achieved the required toughness. A homogeneous microstructure with 170 -181 HV hardness in welding zone, results at this

Table 7. Three Welding joints Hardness Comparison

Welding Current (A)	100 A	150 A	190 A
Ferrite Content	4%	6%	9%
Welding Zone Hardness (HV)	170-181	160-170	150-157
HAZ Hardness (HV)	181-195	165-190	156-185
Hardness Trend	Highest Hardness	Moderate Hardness	Lowest Hardness
Ferrite Impact on Hardness	Higher austenite content leads to higher hardness.	Moderate ferrite leads to moderate hardness.	Highest ferrite content results in lowest hardness.
Cooling Rate and Microstructure Effect	Faster cooling results in finer microstructure and higher hardness.	Moderate cooling results in larger ferrite and coarser microstructure.	Slow cooling allows formation of largest ferrite and coarser microstructure.

Figure 8. Tensile test samples fracture location (A) 100 A, (B) 150 A, and (C) 190 A.

position because of the speeded-up cooling process. The weld zone hardness largely results from austenite when the ferrite content stays within this low value range. The weld material demonstrates tensile strength at 662 MPa and the test samples fracture occurred at the welding zone due to its high hardness and low toughness. The fracture samples as shown in Fig. 8 below illustrated very low elongation, which evidenced the lack with toughness.

Increasing in welding current to 150 A brings about a 6 % ferrite content. A higher heat input with prolonged cooling times enables abundance of ferrite formation because of its slower crystallization process. 6% ferrite presence falls within an acceptable range that maintains advantages like improved toughness even though strength decreases moderately. The welding zone hardness decreases to 160-170 HV as the weld metals contain more ferrite while exhibiting slightly larger grain size. Because ferrite has a reduced hardness in comparison to austenite, it generates overall hardness reduction. The primary composition of the microstructure features austenite that enables the weld to maintain good hardness along with toughness characteristics. This material experiences relatively higher hardness reduction beyond the 100 A-welded metal while staying short of dramatic levels. The tensile strength reaches a value of 689 MPa thereby surpassing the tensile strength of 100 A sample. The this sample fracture location occurred at the HAZ with good elongation as illustrated in Fig. 8 above, the fracture location and type proved the joint high toughness due to the perfect ferrite percentage rang. The austenite-ferrite combination regulates strength properties shown in the material. The minor ferrite enhancement in the metal structure leads to increased toughness and decreased crack vulnerability during stress conditions. The mechanical performance improves because of the ferrite phase added toughness however; ferrite does not control enough of the steel to significantly weaken strength at 6 % content. Ferrite contributes toughness to the weld structure that leads to increased tensile strength while slight reduction in hardness suggests an upcoming trade-off between strength and toughness.

Welding current at 190 A produces excessive ferrite content as the total ferrite reaches 9 %. The weld properties suffer damage from high ferrite content that occurs from excessive ferrite formation because ferrite distributes over the weld as a soft phase that forms a brittle microstructure. The weld tensile strength decreases when ferrite reaches certain thresholds beyond which it constitutes more than a specific percentage. When the weld contains an excessive ferrite amount along with a coarse microstructure, the weld zone hardness reaches levels between 150-157 HV. The presence of increased ferrite in the weld leads to overall softening because ferrite is harder than austenite. This sample fracture location noticed at the welding zone due to the high ferrite percentage and the high cracks susceptibility and formations at this zone under these conditions. The microstructural changes caused by high ferrite content led to reduced hardness because ferrite exhibits less hardness than austenite within the particular alloy composition. The weld's tensile strength diminishes to 677 MPa even though heat input and welding current reached greater levels at 190 A. The weld exhibits a lower strength because the enhancement of ferrite makes the material softer. Too much ferrite within the weld material weakens its tensile force resistance that leads to reduced tensile strength. The weld becomes weaker at 9 % ferrite content regardless of potential increased toughness levels. Ferrite content of 9 % severely damages both weld strength and toughness at 190 A. Higher amounts of ferrite create an excessive weakening effect that decreases tensile strength to 677 MPa. The relationship among welding current, ferrite content, hardness, and tensile strength in the three welding joints summarized in Table 8.

Table 9 below highlights summarized the key parameters and findings of this study.

Table 8. Relationship among welding current, ferrite content, hardness, and tensile strength

Welding Current (A)	Ferrite (%)	Welding Zone Hardness (HV)	HAZ Hardness (HV)	Tensile Strength (MPa)	Fracture location
100	4	170-181	181-195	662	WZ
150	6	160-170	165-190	689	HAZ
190	9	150-157	156-185	677	WZ

Table 9. Key parameters and findings of this study

Welding Current (A)	Ferrite (%)	Welding Zone Hardness (HV)	HAZ Hardness (HV)	Tensile Strength (MPa)	Fracture Location
100 A	4%	170-181	181-195	662	Weld Zone (WZ)
150 A	6%	160-170	165-190	689	Heat Affected Zone (HAZ)
190 A	9%	150-157	156-185	677	Weld Zone (WZ)

RESULTS AND DISCUSSION

The welding current set to 150 A produces an appropriate ferrite content of 6% in welded joints per this research. García-García & Reyes-Calderón (2022) [1] also documented ferrite›s importance for hot cracking prevention in austenitic stainless steel. Your study at 150 A shows improved toughness and reduced cracking rates due to ferrite control as Garcia-Garcia and Reyes-Calderon (2022) [1] demonstrated for the same conditions. The study validates Vasantharaja & Vasudevan›s (2019) [3] research which shows how controlled thermal processes modify ferrite distribution to produce stronger materials. This study demonstrates how interdendritic ferrite formation at moderate heat input (150 A) confirms toughness enhancement. Two studies by mohammed et al. (2017) [13] and Raj et al. (2024) [10] provide strong support for the tensile strength trend that rises with moderate ferrite amounts yet falls with excessive ferrite. Research findings from both studies demonstrate how ferrite content establishes key mechanical properties that guide the behavior of welded joints through their resistance to cracks and overall toughness performance. This study›s hardness evaluation matches prior research showing ferrite content augmentation leads to hardness reduction (Mohammed et al. 2017) [13]. The hardness measurements show decreased values with rising welding currents because ferrite exists as a softer material than austenite yet high levels of ferrite act against hardness development. The relationship between ferrite content and corrosion resistance remains unmeasured in this study but García-García et al. (2022) [1] and Raj et al. (2024) [10] provide evidence that ferrite content affects corrosion resistance. An increase in ferrite content primarily at 190 A alters the material›s resistance to corrosion because the softer ferritic phase has less protection than austenite against corrosion.

CONCLUSION

This research establishes that welding current together with heat input serves as key elements for determining the mechanical properties of TIG-welded AISI 304 stainless steels. The study key finding can be summarized as follow:

1. Welding current elevation produces raised heat input that results in greater ferrite content in the welded area. Endoscopic evaluation showed that the weld ferrite content increased from 4 % at 100 A to 9 % at 190 A based on Schaeffler diagram predictions. The welding current affects the heat input that causes the ferrite content to rise.
2. Using a low heat input of 100 A causes the weld to cool quickly thus producing a fine-grained microstructure of low ferrite content. The strength becomes very high but solidification cracking emerges as a vulnerability. The welding process that produces Moderate Heat Input requires (150 A) as its setting because moderate cooling allows the weld to develop austenite and ferrite in a balanced microstructure. The combination of these elements leads to higher tensile strength in addition to better crack protection. Welds cooled slowly at 190 A heat input since it creates coarsened grains along with an excess of ferrite thus weakening the weld strength. Lower strength and hardness result from welding with this current endpoint.
3. The highest hardness (170-181 HV) appears in 100 A (4% ferrite) welds across the weld area and heat affected zone because austenite dominates while being harder than ferrite. A greater amount of ferrite enhances the endurance qualities and reduces cracking tendencies of the welded material. A hardness reduction occurs when ferrite exceeds 9 % in 190 A welds thus making the weld zone reach 150-157 HV. The appearance of additional ferrite elements inside the weld creates softness that afterward leads to reduced hardness because ferrite possesses low hardness values.

4. When the weld reaches 100 A (4 % ferrite composition) its tensile strength reaches 662 MPa after evaluation. The good strength characteristics of the weld come from its high austenite content. Welded material strength rises to 689 MPa when measured at 150 A because of 6 % ferrite. Ferrite enhancement brings better toughness but weaker tensile strength to welds because ferrite has a softer material quality. Tensile strength drops to 677 MPa at 190 A (9 % ferrite). The weld achieves reduced tensile strength because of the high welding current that creates excessive ferrite content that makes the weld softer. The occurrence demonstrates that elevating welding currents fails to ensure weld strength improvement.
5. The optimal welding current at 150 A produces 6 % ferrite in the welding joint that delivers the ideal combination of strength with toughness and corrosion resistance attributes. A maximum mechanical performance combined with crack resistance makes this current the best selection for welding applications. When using 100 A welding current the weld shape becomes predominantly austenitic leading to strong applications but shows reduced toughness alongside increased hot cracking tendencies whereas 190 A welding current produces excessive ferrite formation that softens the weld and weakens tensile strength despite higher weld temperature. Internal use of the welding technique should be limited for applications that need superior strength since it helps reduce cracking but weakens material properties.
6. This study examines the impact of varying TIG welding currents (100 A, 150 A, and 190 A) on the ferrite content and microstructure of AISI 304 stainless steel welds. The approach examines the impact of variations in welding currents on ferrite levels and the implications of these levels for the future characteristics and durability of weld. The ferrite concentration was shown to rise with increasing welding current, rising from 4% at 100 A to 9% at 190 A. Welding test indicated that a current of 150 A yielded the most advantageous mechanical qualities, namely a high tensile strength (689 MPa), a moderate hardness level (about 160-170 HV), and robust resistance to hot cracking. While low levels of ferrite enhance the steel›s protection, a concentration of 9% or over at 190 A diminishes its strength, rendering it unsuitable for applications demanding higher strength. Experts believe that welding at 150 A produces a product that is durable, robust, and resistant to corrosion, with less risk of hot cracking.

AUTHORSHIP CONTRIBUTIONS

Authors equally contributed to this work.

DATA AVAILABILITY STATEMENT

The authors confirm that the data that supports the findings of this study are available within the article. Raw data that support the finding of this study are available from the corresponding author, upon reasonable request.

CONFLICT OF INTEREST

The author declared no potential conflicts of interest with respect to the research, authorship, and/or publication of this article.

ETHICS

There are no ethical issues with the publication of this manuscript.

STATEMENT ON THE USE OF ARTIFICIAL INTELLIGENCE

Artificial intelligence was not used in the preparation of the article.

REFERENCES

[1] García-García V, Reyes-Calderón F, Frasco-García OD, Alcantar-Modragón N. Mechanical behavior of austenitic stainless-steel welds with variable content of δ-ferrite in the heat-affected zone. Eng Fail Anal 2022;140:106618. [CrossRef]

[2] Chukwuneke JL, Ndefo MI, Sinebe JE, Ofochebe SM. Numerical and thermal analysis of mechanical properties degradations and distortions in steel weld joint. Clean Mater 2022;6:100150. [CrossRef]

[3] Vasantharaja P, Vasudevan M, Parameswaran P. Effect of welding techniques on the microstructure and mechanical properties of reduced activation ferritic-martensitic (RAFM) steel weld joints. Fusion Eng Des 2019;148:111289. [CrossRef]

[4] Han Y, Chu J, Wang Q, Fu K, Jin H, Wei Y. Investigation of microstructure, mechanical properties, residual stress, and distortion in multi-pass gas metal arc welding of ZGMn13Mo/A514 dissimilar joints. Mater Chem Phys 2025;341:130941. [CrossRef]

[5] Sonar T, Ivanov M, Trofimov E, Liu K, Shcherbakov I, Shaburova N, et al. A critical review on dissimilar welding of ferritic-martensitic steel and austenitic stainless steel using gas tungsten arc welding process: Weldability issues, processing, and performance characteristics of joints. J Manuf Process 2025;133:811-864. [CrossRef]

[6] Fei Z, Pan Z, Cuiuri D, et al. Effect of post-weld heat treatment on microstructure and mechanical properties of deep penetration autogenous TIG-welded dissimilar joint between creep strength enhanced ferritic steel and austenitic stainless steel. Int J Adv Manuf Technol 2020;108:3207-3229. [CrossRef]

[7] Queiroz AVD, Fernandes MT, Silva L, Demarque R, Xavier CR, Castro JAD. Effects of an external magnetic field on the microstructural and mechanical properties of the fusion zone in TIG welding. Metals 2020;10(6):714. [CrossRef]

[8] Li J, Li H, Peng W, Xiang T, Xu Z, Yang J. Effect of simulated welding thermal cycles on microstructure and mechanical properties of coarse-grain heat-affected zone of high nitrogen austenitic stainless steel. Mater Charact 2019;149:206-217. [CrossRef]
[9] Maduraimuthu V, Vasudevan M, Muthupandi V, et al. Effect of activated flux on the microstructure, mechanical properties, and residual stresses of modified 9Cr-1Mo steel weld joints. Metall Mater Trans B 2012;43:123-132. [CrossRef]
[10] Raj CR, Kumar S, Chandra K, Roychowdhury S, Singh PK. Thermal aging effects on tensile and metallurgical characteristics of stainless steel weld joint. Procedia Struct Integr 2024;60:709-722. [CrossRef]
[11] Zmitrowicz P, Kawiak M, Kochmański P, Baranowska J. Microstructure and mechanical properties of welded joints of 1.4462 duplex steel made by the K-TIG method. Materials 2021;14:7868. [CrossRef]
[12] Noga P, Skrzekut T, Wędrychowicz M, Węglowski MS, Wiewióra M. The influence of various welding methods on the microstructure and mechanical properties of 316Ti steel. Materials 2024;17(7):1681. [CrossRef]
[13] Mohammed GR, Ishak M, Aqida SN, Abdulhadi HA. Effects of heat input on microstructure, corrosion and mechanical characteristics of welded austenitic and duplex stainless steels: A review. Metals 2017;7(2):39. [CrossRef]
[14] Higelin A, Le Manchet S, Passot G, et al. Heat-affected zone ferrite content control of a duplex stainless steel grade to enhance weldability. Weld World 2022;66:1503-1519. [CrossRef]
[15] Wang P, Szalowski B, Vallant R, Poletti C, Enzinger N. Influence of thermomechanical treatments on the microstructure and mechanical properties of AISI 304L welds. Weld Int 2023;37(2):79-90. [CrossRef]
[16] Hu Y, Shi Y, Wang K, Huang J. Effect of heat input on the microstructure and mechanical properties of local dry underwater welded duplex stainless steel. Materials 2023;16(6):2289. [CrossRef]
[17] Zhang J, Cui K, Huang B, Mao XD, Zheng MJ. Influence of heat input on the microstructure and mechanical properties of CLAM steel multilayer butt-welded joints. Fusion Eng Des 2020;152:111413. [CrossRef]
[18] Babu PD, Gouthaman P, Marimuthu P. Effect of heat sink and cooling mediums on ferrite austenite ratio and distortion in laser welding of duplex stainless steel 2205. Chin J Mech Eng 2019;32:50. [CrossRef]
[19] Polish Committee for Standardization. PN-EN ISO 5173:2010; Destructive testing of welds in metal materials—Bending test. Warsaw, Poland: Polish Committee for Standardization; 2010.
[20] Polish Committee for Standardization. PN-EN ISO 6507-2:2018-05; Metals—Vickers hardness measurement. Warsaw, Poland: Polish Committee for Standardization; 2018.
[21] Devendranath Ramkumar K, Pavan B, Chandrasekar V. Development of improved microstructural traits and mechanical integrity of stabilized stainless steel joints of AISI 321. J Manuf Process 2018;32:582-594. [CrossRef]
[22] ASTM E8 / E8M-24, Standard Test Methods for Tension Testing of Metallic Materials, ASTM International, West Conshohocken, PA, 2024.
[23] Dauod DS, Mohammed MS, Aziz IAA, Abbas AS. Mechanical vibration influence in microstructural alterations and mechanical properties of 304 stainless steel weld joints. J Eng Sci Technol 2023;(Special Issue 6):33-54.
[24] Lai CL, Tsay LW, Kai W, Chen C. The effects of cold rolling and sensitisation on hydrogen embrittlement of AISI 304L welds. Corros Sci 2010;52:1187-1193. [CrossRef]
[25] Klimpel A. The influence of alloying elements on the formation of the sigma phase in austenitic-ferritic weld metals type 18-8. Sci Noteb Mech Silesian Univ Technol 1977;509:1-85.
[26] Kou, S. (2003). Welding Metallurgy (2nd ed.). John Wiley & Sons.
[27] Kulkarni A, Dwivedi DK, Vasudevan M. Microstructure and mechanical properties of A-TIG welded AISI 316L SS-Alloy 800 dissimilar metal joint. Mater Sci Eng A 2020;790:139685. [CrossRef]
[28] Kou S. Welding Metallurgy. Hoboken, NJ, USA: John Wiley & Sons; 2003.
[29] Amin SA, Abdulhasan AA, Mohammed MS, Majdi HS. Experimental and numerical study of maximum welding joint temperature impacts in alloy steel pipe welding microstructure, distortion, corrosion resistance, and mechanical properties. Rev Compos Mater Av-J Compos Adv Mater 2024;34(6):775-786. [CrossRef]
[30] Eid A, Abd Allatif M, Elsabbagh A, Halfa H. Effect of heat input on weldability of low nickel high manganese stainless steel. Int J Mater Technol Innov 2023;3(2):19-29. [CrossRef]
[31] Kim YH, Kim DG, Sung JH, et al. Influences of Cr/Ni equivalent ratios of filler wires on pitting corrosion and ductility-dip cracking of AISI 316L weld metals. Met Mater Int 2011;17:151-155. [CrossRef]
[32] Yamashita S, Ike K, Yamasaki K, et al. Relationship between ferrite–austenite phase transformation and precipitation behavior of sigma phase in super duplex stainless steel weldment. Weld World 2022;66:351-362. [CrossRef]
[33] Guilherme LH, Benedetti AV, Fugivara CS, Magnabosco R, Oliveira MF. Effect of MAG welding transfer mode on sigma phase precipitation and corrosion performance of 316L stainless steel multipass welds. J Mater Res Technol 2020;9(5):10537-10549. [CrossRef]

[34] Dauod DS, Wade KJ, Mohammed MS, Majdi HS. Analysis of shielding gases influences 304 gas metal arc welding microstructure, weld geometry, and mechanical properties. Rev Compos Mater Av-J Compos Adv Mater 2024;34(4):435-446. [CrossRef]

[35] Hsieh CC, Guo X, Chang CM, et al. Dendrite evolution of delta (δ) ferrite and precipitation behavior of sigma (σ) phase during multipass dissimilar stainless steels welding. Met Mater Int 2010;16:349-356. [CrossRef]

[36] Dewangan S, Saksham S. Analysis among quenched, tempered, and stepped cooled TIG welded SS-304 plates based on tensile strength, hardness, and microstructural appearance. Adv Mater Sci Eng 2023;2023:5523162. [CrossRef]